Nanocrystals of metals, semiconductors and oxides: Novel synthesis and applications*

C. N. R. Rao[†,#,], G. U. Kulkarni[†], P. John Thomas[†], Ved Varun Agrawal[†], Ujjal K. Gautam[†,#] and Moumita Ghosh[†,#]**

[†]Chemistry and Physics of Materials Unit, Jawaharlal Nehru Centre for Advanced Scientific Research, Jakkur, P.O., Bangalore 560 064, India
[#]Solid State and Structural Chemistry Unit, Indian Institute of Science, Bangalore 560 012, India

Films of nanocrystals such as Au, Ag and Pd, semiconducting sulphides such as CdS, ZnS and CoS, and oxides such as Fe_2O_3 and CuO have been prepared by employing reactions at liquid–liquid (organic–aqueous) interfaces. In this method, a suitable organic derivative of the metal taken in the organic layer reacts at the interface with the appropriate reagent present in the organic layer. Two typical applications of nanocrystals pertaining to magnetic devices and dip-pen lithography are briefly presented.

THE synthesis and characterization of nanocrystals of materials have become an area of intense research activity over the last few years[1–11]. Several methods have been reported for the preparation of nanocrystals of metals such as Au and Ag and of semi-conductors such as CdS and CdSe[7–11]. Thus, metal nanocrystals are generally obtained by the controlled reduction of metal salts, while nanocrystals of metal chalcogenides and oxides are prepared by arrested precipitation or thermal decomposition[1–6]. Although much has been achieved in controlling the size distribution of nanocrystals, it has often been difficult to obtain robust films of nanocrystals through self-assembly. Producing nanocrystal films by molecular beam epitaxy and other physical methods often tends to be tedious and equipment-intensive. We have made use of the interface between two immiscible liquids to prepare nanocrystals of metals, semiconductors and metal oxides as well as thin films of these materials. In this method, the organic layer containing the metal precursor comes into contact with the aqueous layer containing a suitable reagent for reduction, hydrolysis or sulphidation. The reaction occurs at the interface, depositing the nanocrystals at the interface, the yield and the size distribution depending on the reaction parameters such as reagent concentration, mode of dispersal of reagents, mechanical agitation, temperature and viscosity of the medium. By an appropriate choice of the reaction parameters, we can obtain isolated nanocrystals with a narrow size distribution or well-formed films of the nanocrystals. It is noteworthy that the present method is distinct from the methods where a phase boundary is used to slow down diffusion to another medium[7]. In this communication we briefly present typical results obtained by this method to illustrate its versatility.

Nanocrystals of metals and semiconductors are finding a variety of applications starting from biological tagging to electronic devices. We present preliminary results of our study of *g*-Fe_2O_3 nanocrystalline films to explore anisotropic magnetization, and of aqueous dispersions of metal nanocrystals as inks in dip-pen lithography.

In order to prepare nanocrystals of Au, the triphenyl phosphine derivative of the metal ($Au(PPh_3)Cl$) was dispersed in the toluene layer and the reducing agent, tetrakishydroxymethylphosphonium chloride[11,12] was injected into the aqueous layer containing alkali. Figure 1 *a* shows how the reaction carried out at 298 K was confined exclusively to the liquid–liquid interface. Examination of the films at the interface by transmission electron microscopy (TEM) revealed that they consisted of close-packed Au nanocrystals. In Figure 2, we show TEM images of the Au nanocrystals obtained with two different concentrations of $Au(PPh_3)Cl$. We observe that with increase in the concentration of the metal precursor we get films of

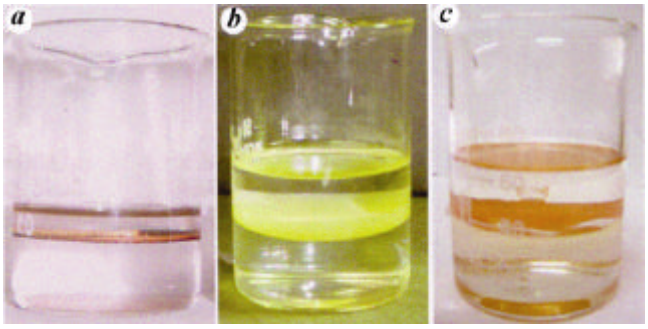

Figure 1. Nanocrystals of (***a***) Au, (***b***) CdS and (***c***) *g*-Fe_2O_3 formed at the toluene–water interface.

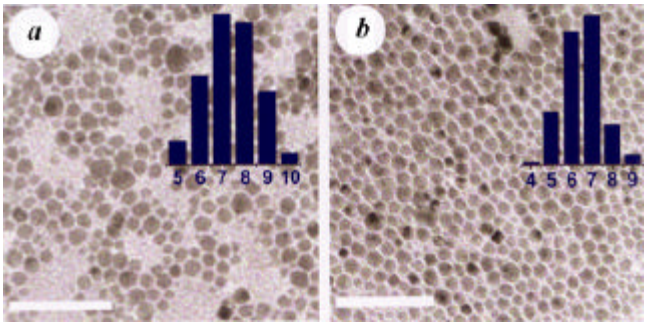

Figure 2. ***a***, TEM image of the as-prepared Au nanocrystals obtained after 24 h from a liquid–liquid interface containing a 1.5 mM solution of $Au(PPh_3)Cl$ in toluene and 330 µl of 50 mM THPC in 16 ml of 6.25 mM aqueous NaOH solution in a 50 ml beaker (bar = 50 nm). ***b***, TEM image of Au nanocrystals obtained starting with a 6 mM toluene solution of $Au(PPh_3)Cl$ and 1.65 ml of 50 mM THPC in 16 ml of 31.25 mM aqueous NaOH solution (bar = 50 nm). (Inset) Particle size distribution (in nm).

*Dedicated to Prof. S. Ramaseshan on his 80th birthday.
**For correspondence. (e-mail: cnrrao@jncasr.ac.in)

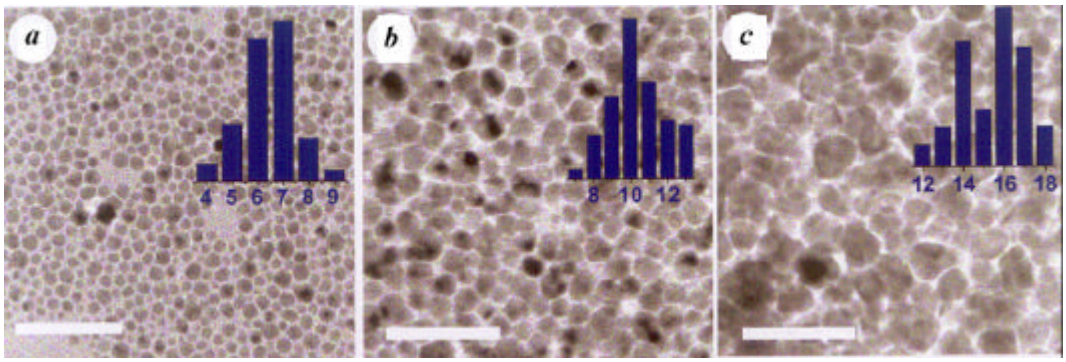

Figure 3. ***a***, TEM image of Au nanocrystals obtained at room temperature from a liquid–liquid interface containing a 1.5 mM toluene solution of $Au(PPh_3)Cl$ and 330 µl of 50 mM THPC in 16 ml of 6.25 mM aqueous NaOH solution in a 50 ml beaker (bar = 50 nm). TEM image of (***b***) particles obtained at 323 K (bar = 50 nm) and (***c***) particles obtained at 348 K (bar = 50 nm). (Inset) Size distributions of the particles.

nanocrystals with more number of particles, but the size distribution is not greatly effected. Use of a low concentration of the metal precursor results in some metal nanoparticles in the aqueous layer below the film at the interface, while a high concentration of the metal precursor gives metal nanoparticles in the organic layer. We obtain films of metal nanoparticles only at the interface, leaving both the liquid layers clear, only when an optimal precursor concentration is employed.

The temperature of the reaction has a marked effect on the size distribution of the Au nanocrystals, as can be seen from the TEM images in Figure 3. When the reaction is carried out at different temperatures in a hot-air oven, the average particle size varies from 7 nm at 298 K to 16 nm at 348 K. We have examined the effect of viscosity of the aqueous layer on particle size distribution by adding glycerol to the aqueous layer. The particle size decreases significantly as the proportion of glycerol and the associated viscosity of the aqueous layer increases. TEM images in Figure 4 clearly demonstrate the effect of viscosity.

By employing high concentration of metal precursors, lustrous thin films of gold of varying thickness could be prepared. The films are readily transferred to a solid substrate by raising the substrate gently across the interface. Preliminary cross-sectional scanning electron microscopic and atomic force microscopic (AFM) investigations reveal that the thickness of the films varies in the range of 80–1000 nm on varying the concentration of the precursors. Tapping mode AFM studies show the presence of aggregates of granules in the films with a rms roughness of 35 nm (Figure 5).

An important feature of the liquid–liquid interface method is that the nanocrystals at the interface can be transferred to either the aqueous or the organic phase using appropriate capping agents. For example, by the addition of dodecanethiol to the organic layer, the Au nanocrystals could be transferred entirely to the organic layer, while the addition of mercaptoundecanoic acid transferred the nanocrystals to the aqueous layer. The

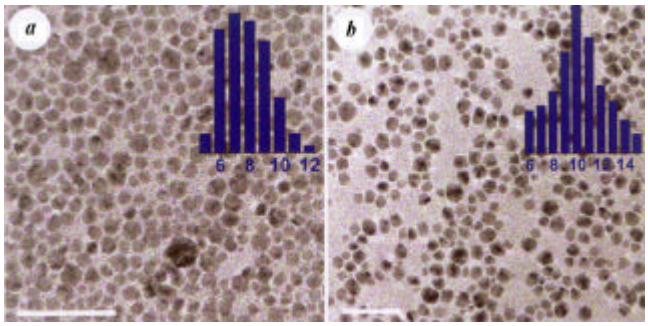

Figure 4. ***a***, TEM image of Au particles obtained at room temperature by reacting a THPC solution in a 3 : 1 water–glycerol mixture and $Au(PPh_3)Cl$ in toluene layer (bar = 50 nm). ***b***, TEM image of Au particles obtained at room temperature by reacting a THPC solution in a 1 : 1 water–glycerol mixture and $Au(PPh_3)Cl$ in toluene layer (bar = 50 nm). (Inset) Particle size distributions.

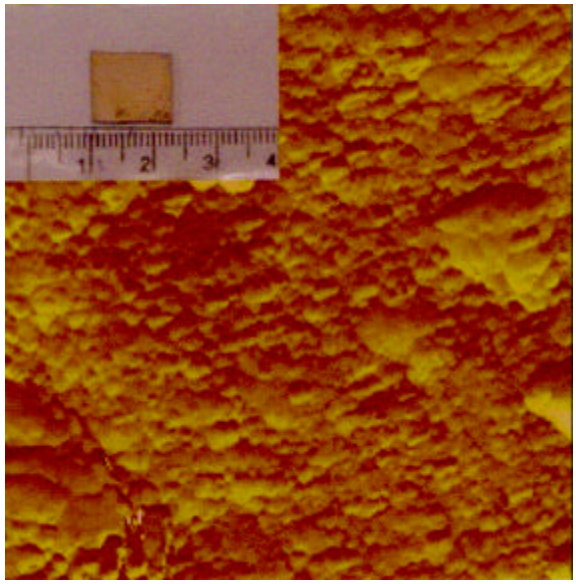

Figure 5. Tapping mode atomic force microscopic image (in phase contrast mode) of an Au film transferred to a highly oriented pyrolytic graphite substrate. The film was prepared starting with 10 mM solution of $Au(PPh_3)Cl$ in toluene. (Inset) Similar film on a glass substrate.

transfer of the Au nanocrystals to the aqueous or the organic medium is marked by the acquisition of a vivid colour by the respective layer, as demonstrated in Figure 6. There is little change in the average diameter of the nanocrystals after transfer to the organic or the aqueous medium from the interface.

We have been able to obtain nanocrystals of other metals such as silver and palladium as well, by employing the liquid–liquid interface. In Figure 7, we show a TEM image of the small Pd nanocrystals obtained by reacting a dispersion of palladium acetate in the toluene layer with THPC in the aqueous layer.

We have attempted to characterize the metal nanocrystal films obtained at the interface by electrical-resistivity measurements. We observe different resistivity behaviours in the films prepared at different temperatures and concentrations. For example, films of Au obtained at 298 K show a non-metallic behaviour of resistivity, while the ones prepared at 348 K exhibit metallic behaviour. A study of the transport properties of the films prepared under different reaction conditions is currently in progress, in order to relate the structure of the film with the resistivity behaviour.

The universality of the use of the liquid–liquid interface for the synthesis of nanocrystals is demonstrated by the successful synthesis of CdS and other metal sulphide nanocrystals. That the reaction occurs at the interface in these cases as well can be seen clearly from Figure 1 *b*. CdS nanocrystals with an average diameter of ~ 5 nm were obtained by reacting cadmium cupferronate in the toluene layer with Na_2S in the water layer at 298 K (Figure 8 *a*). The particles exhibit the blue-shifted absorption band at 450 nm (bulk value 515 nm). CdS nanocrystals of ~ 8 nm diameter were obtained by carrying out the reaction at 353 K. This method could be readily extended to prepare films of nanocrystalline CoS, NiS, CuS and ZnS. In Figure 8 *b*, we show the TEM image of CoS nanocrystals obtained by reacting cobalt stearate in the toluene layer with Na_2S in the aqueous layer.

Nanocrystals of *g*-Fe_2O_3 with a diameter of ~ 2.6 nm were obtained by reacting iron cupferronate in the toluene layer with NaOH in the water layer (Figure 9 *a*). The

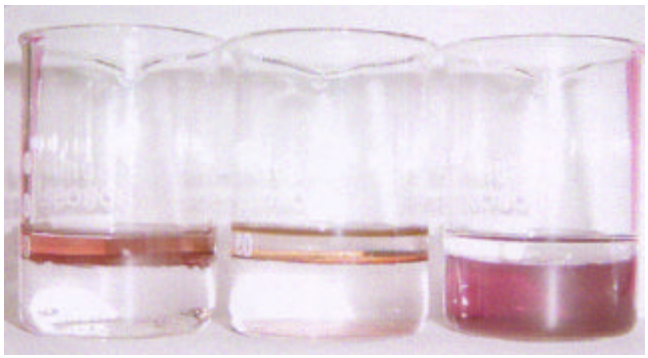

Figure 6. (Middle) Nanocrystals of Au formed at the toluene–water interface. (Left) When dodecanethiol is added to the toluene layer, the Au nanocrystals form an organosol. (Right) When mercaptoundecanoic acid is added to the water layer, the Au nanocrystals produce a hydrosol.

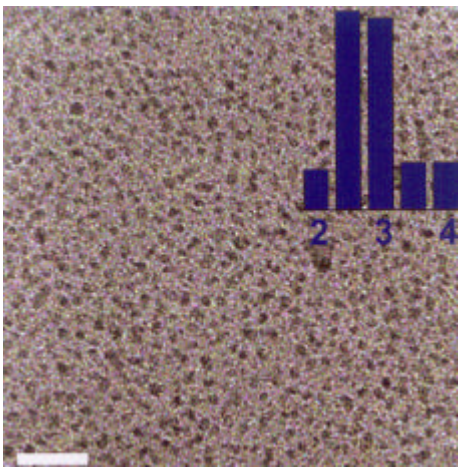

Figure 7. TEM image of Pd nanocrystals obtained at room temperature by reacting a 2.2 mM toluene dispersion of palladium acetate with 330 µl of 50 mM THPC in 16 ml of 6.25 mM aqueous NaOH solution in a 50 ml beaker (bar = 20 nm). (Inset) Particle size distribution.

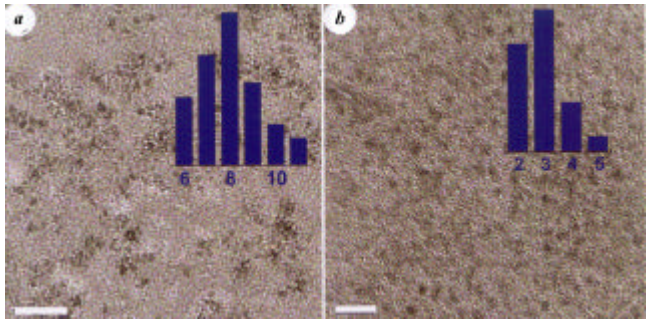

Figure 8. ***a***, TEM image of CdS nanocrystals (~ 8 nm average diameter) prepared at the water–toluene interface. The sample was prepared by treating 0.05 mM solution of cadmium cupferronate in toluene with 0.10 mM aqueous Na_2S for 12 h (bar = 50 nm). ***b***, TEM image of CoS nanocrystals (~ 3 nm average diameter) prepared at the water–toluene interface using the same concentration of starting materials as that of CoS (bar = 10 nm).

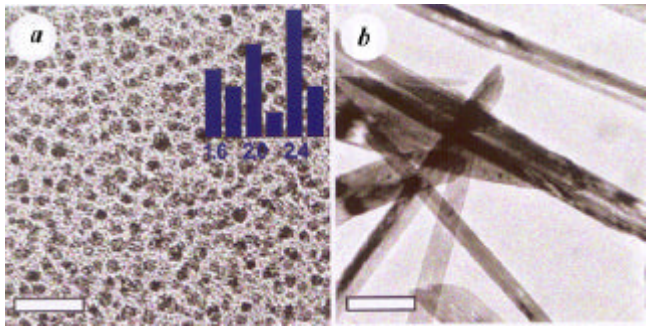

Figure 9. ***a***, *g*-Fe_2O_3 nanocrystals (~ 2.6 nm average diameter) obtained from a interface film, starting with 0.0428 mM iron(III) cupferronate solution in toluene, allowing it to react with 1.87 mM aqueous NaOH for 8 h at room temperature. The nanocrystals are quite monodisperse in nature (bar = 10 nm). ***b***, CuO nanorods obtained by reacting a dispersion of 0.02 g of $Cu(cup)_2$ in toluene with 20 ml 1N NaOH solution for 36 h (bar = 200 nm).

g-Fe_2O_3 particles are superparamagnetic. ZnO nanocrystals and nanorod-like structures exhibiting a blue-shifted luminescence could be prepared starting with zinc cupferronate in the organic layer and NaOH in the aqueous layer. Similarly, using a dispersion of copper cupferronate in the toluene layer and with NaOH in the aqueous layer, nanorods of CuO have been obtained. Figure 9 *b* shows the TEM image of CuO nanorods. This method can clearly be extended to prepare other metal-oxide nanocrystals as well.

Films of g-Fe_2O_3 nanocrystals of various thicknesses were deposited on solid substrates by successive addition of dispersions of the nanocrystals in toluene or in water. Films of citrate-capped g-Fe_2O_3 prepared by us on Si(100) substrates were smooth, extending to several microns. Tapping-mode AFM images reveal that the films are composed of ~ 12 nm diameter nanoparticles. The films were magnetic showing hysteresis, unlike the nanoparticles which were only superparamagnetic. Magnetic measurements were carried out along two different orientations of the film (Figure 10). Interestingly, the films show preferential perpendicular ordering of the easy magnetic axis (Figure 11). Thus, the coercivity is larger in the perpendicular orientation. Small perpendicular magnetization exhibited by the nanocrystal films is of great value in magnetic recording and other applications[13].

We have found that the nanocrystals of metals such as gold dispersed in water can be used for nanolithography by the dip-pen process[14]. In this technique, Au nanocrystals deposited on the AFM cantilever dissolve in the water meniscus between the tip and the substrate (Figure 12). The dissolved nanocrystals are transferred to the substrate when the tip is slowly scanned over the surface. Aggregates of the nanocrystals are formed on the substrate upon evaporation of the water layer. In Figure 13, we show the AFM image of a line (35 nm × 750 nm) drawn in this manner along with a plot of the cross-sectional profile. The small width of the line obtained by this method is gratifying.

The liquid–liquid interface promises to be a universal medium for the synthesis of nanocrystals and thin films of a variety of materials. The results obtained so far fully support such an expectation. The various subtle reaction parameters permit the required control over the size distri-

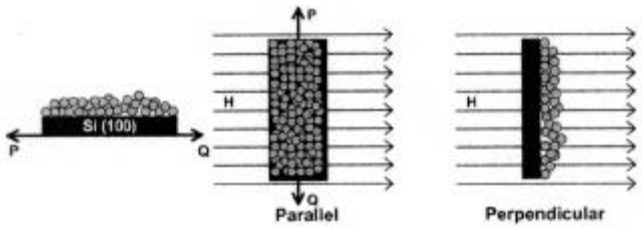

Figure 10. Schematic illustration of the two different orientations of g-Fe_2O_3 nanocrystalline films along which magnetic measurements were carried out. Change in the orientation was brought about by rotating the film along the *PQ* axis.

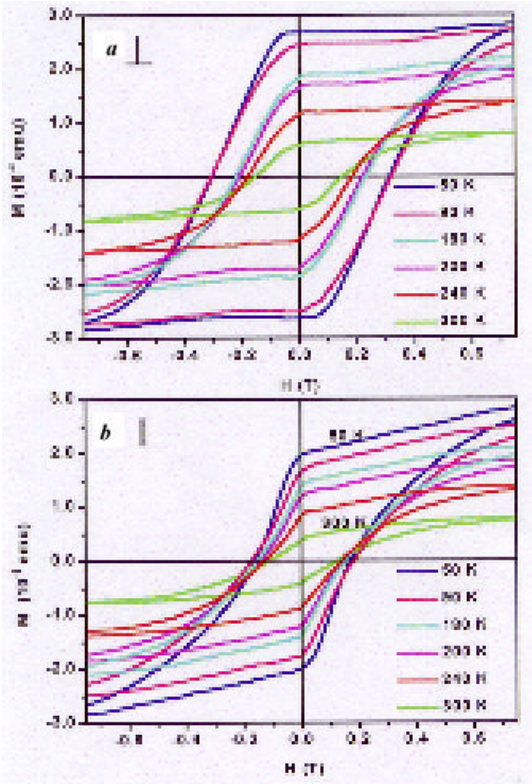

Figure 11. Hysteresis loops from a citrate-capped g-Fe_2O_3 film at various temperatures with the substrate held (***a***) perpendicular and (***b***) parallel to the applied field direction. Note that the hysteresis loops are steeper and wider in the perpendicular orientation.

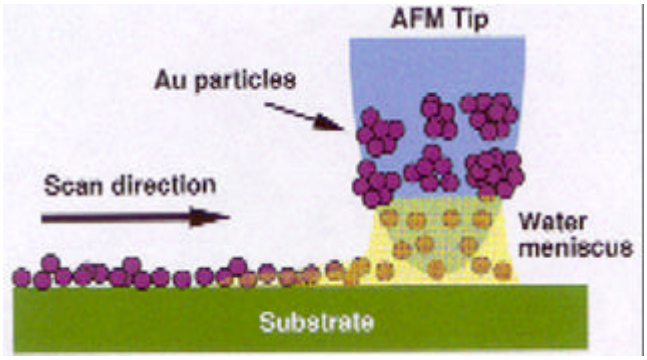

Figure 12. Schematic illustration of the dip-pen process. Au nanocrystals deposited on the cantilever dissolve in the water meniscus between the tip and the substrate. The dissolved nanocrystals are transferred to the substrate, when the tip is slowly scanned across the surface. Aggregates of nanocrystals are formed on the substrate upon evaporation of the water layer.

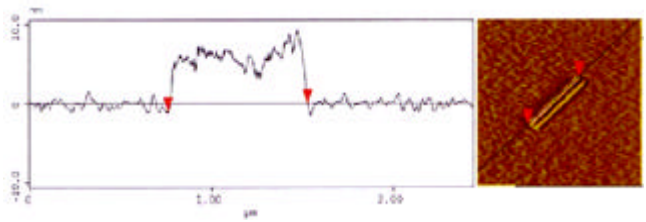

Figure 13. A plot of the cross-sectional profile along a line made of Au nanocrystals shown in the AFM image. The area plotted is indicated in the AFM image alongside.

bution and properties of the nanocrystals obtained by this method. Two potential applications of nanocrystals have been demonstrated, one dealing with perpendicular magnetization of g-Fe_2O_3 films and the other with nanolithography using Au nanocrystals.

1. Schmid, G., *Clusters and Colloids: From Theory to Applications*, Wiley-VCH, Weinheim, 1994.
2. Fendler, J. H., *Nanoparticles and Nanostructured Films Preparation, Characterization and Applications*, Wiley-VCH, Weinheim, 1998.
3. Rao, C. N. R., Kulkarni, G. U., Thomas, P. J. and Edwards, P. P., Size-dependent chemistry: Properties of nanocrystals. *Chem. Eur. J.*, 2002, **8**, 29–35.
4. Trindade, T., O'Brien, P. and Pickett, N. L., Nanocrystalline semiconductors: synthesis, properties and perspectives. *Chem. Mater.*, 2001, **13**, 3843–3558; Esteves., A. C. C. and Trindade, T., Synthetic studies on II/VI semiconductor quantum dots. *Curr. Opinion Solid State Mater. Sci.*, 2002, **6**, 347–353.
5. Green, M., Solution routes to III–V semiconductor quantum dots. *Curr. Opinion Solid State Mater. Sci.*, 2002, **6**, 355–363.
6. Pileni, M.-P., The role of soft colloidal templates in controlling the size and shape of inorganic nanocrystals. *Nature Mater.*, 2003, **2**, 145–150.
7. Brust, M., Bethell, D., Schiffrin, D. J. and Kiely, C. J., Novel gold-dithiol nano-networks with non-metallic electronic properties. *Adv. Mater.*, 1995, **7**, 795–797.
8. Rockenberger, J., Scher, E. J. and Alivisatos, A. P., A new non-hydrolytic single precursor approach to surfactant-capped nanocrystals of transition metal oxides. *J. Am. Chem. Soc.*, 1999, **121**, 11595–11596.
9. Murray, C. B., Norris, D. J. and Bawendi, M. G., Synthesis and characterization of nearly monodisperse CdE (E = sulfur, selenium, tellurium) semiconductor nanocrystallites. *J. Am. Chem. Soc.*, 1993, **115**, 8706–8715.
10. Sarathy, K. V., Kulkarni, G. U. and Rao, C. N. R., A novel method of preparing thiol-derivarised nanoparticles of gold, platinum and silver forming superstructures. *J. Chem. Soc., Chem. Commun.*, 1997, 537–538.
11. Duff, D. G., Baiker, A. and Edwards, P. P., A new hydrosol of gold clusters. 1. Formation and particle size variation. *Langmuir*, 1993, **9**, 2301–2309.
12. Duff, D. G., Baiker, A., Gameson, I. and Edwards, P. P., A new hydrosol of gold structures. 2. A comparison of some different measurement techniques. *Langmuir*, 1993, **9**, 2310–2317.
13. Zeng, H., Li, J., Liu, J. P., Wang, Z. L. and Sun, S., Exchange-coupled nanocomposite magnets by nanoparticle self-assembly. *Nature*, 2002, **420**, 395–398; Sun, S., Murray, C. B., Weller, D., Folks, L. and Moser, A., Monodisperse FePt nanoparticles and ferromagnetic FePt nanocrystal superlattices. *Science*, 2000, **287**, 1989–1992; Ngo, A. T. and Pileni, M. P., Assemblies of ferrite nanocrystals: Partial orientation of the easy magnetic axes. *J. Phys. Chem. B*, 2001, **105**, 53–58.
14. Demers, L. M. and Mirkin, C. A., Combinatorial templates generated by dip-pen nanolithography for the formation of two-dimensional particle arrays. *Angew. Chem., Int. Ed. Engl.*, 2001, **40**, 3069–3071.

ACKNOWLEDGEMENTS. We thank the DRDO and the Department of Science and Technology for support. U.K.G. thanks CSIR for a senior research fellowship.

Received 8 September 2003

Structural and dynamical consequences on various high-pressure phase transitions in laser host fluoroscheelites $LiYF_4$ and $LiYbF_4$*

A. Sen, S. L. Chaplot† and R. Mittal

Solid State Physics Division, Bhabha Atomic Research Centre, Trombay, Mumbai 400 085, India

Computer simulations of pressure-induced phase transitions in $LiYF_4$ and $LiYbF_4$ have been carried out using complementary techniques of molecular dynamics (MD) and lattice dynamics. The MD simulations at a constant temperature of 300 K with increasing pressure reveal structural changes at around 5 and 15 GPa and the crystallographic space groups of the new structures. The lattice dynamics calculations are then conveniently used to derive the vibrational spectra and the free energies and its consequences on the thermodynamic stability of the new phases.

IN recent years, lithium rare earth fluoroscheelites such as $LiYF_4$ and $LiYbF_4$ have been studied extensively[1–16] with a view to better-understand their thermal and optical properties that are exhibited upon doping with trivalent rare-earth ions (e.g. Nd^{3+}, Ho^{3+}, Eu^{3+}, etc.) in a wide range (UV–IR) of highly efficient lasing actions. Both $LiYF_4$ and $LiYbF_4$ crystallize under ambient conditions in the tetragonal scheelite structure (space group: $I4_1/a$, $Z = 4$), with two molecules in the unit cell[6]. Although isostructural with oxoscheelites (viz. $CaWO_4$), these compounds have different pressure responses compared to that of the former, making them worthy for further study, especially in areas of high-pressure phase transitions.

As we know, pressure reduces the volume of a substance, thereby causing significant changes in its electronic and vibronic states, chemical bonding and atomic packing. Hence, investigations of pressure-dependent optic and thermodynamic properties often yield invaluable information on many properties of materials at high pressures. Pressure-dependent Raman study by Sarantopoulou *et al.*[10] has already pointed out an abrupt change of slope in the frequency versus pressure diagrams of phonon modes at 7 GPa, signifying the onset of structural instabilities in $LiYF_4$ with increase in pressure. This observation was supported by our previous lattice-dynamical work[11], where we have shown the splitting of B_g/E_g Raman lines in the vicinity of 350 and 400 cm^{-1}. We further attribute the initiation of discontinuities in the Raman spectra of $LiYF_4$ to the softening of transverse acoustic phonon modes in the direction of dynamical insta-

*Dedicated to Prof. S. Ramaseshan on his 80th birthday.

†For correspondence. (e-mail: chaplot@magnum.barc.ernet.in)